AIAA SciTech Forum
January 3-7, 2022, San Diego, CA & Virtual
AIAA SCITECH 2022 Forum

10.2514/6.2022-0988

Development of the Focused Malley Probe as a Local Aero-Optical Measurement Technique

Luke Butler[1] and Stanislav Gordeyev[2]
University of Notre Dame, Notre Dame, IN, 46556

A novel local aero-optical measurement technique, termed the focused Malley probe, is presented, where two converging-diverging laser beams passing through a wind tunnel are used to perform localized aero-optical jitter and convective speed measurements. Validating experiments were conducted using a subsonic speed tunnel with a small diameter cylinder placed in the middle of the test section to create local aero-optical distortions in the wake downstream. Measurements were performed in the wake downstream of the cylinder, in the freestream upstream of the cylinder, and in the turbulent boundary layer upstream of the cylinder. Spectral analysis of the cross-correlations between two beams in these preliminary experiments clearly demonstrate the ability of the focused Malley probe under certain conditions to measure convective velocity primarily near the focal point. In the case when the focal points were placed inside the cylinder's wake, a spectral peak corresponding to the shedding frequency was clearly resolved despite the presence of the corrupting effects from the boundary layers at the walls of the tunnel. Various experimental and data processing requirements to obtain accurate results are also discussed.

I. Introduction

As a laser beam passes through turbulent flow, aero-optical structures of fluctuating densities impose optical aberration on the beam and, among other things, will cause the beam to propagate in a different direction. This is known as beam deflection or beam jitter. For small beam diameters, Huygens principle states [1] that the beam will be deflected by an amount proportional to the 2-D gradient of optical path length (OPL), according to,

$$\theta_x(t) = \frac{\partial}{\partial x} OPL(x,y,t),\ \theta_y(t) = \frac{\partial}{\partial y} OPL(x,y,t),$$

as schematically shown in Figure 1. OPL, in turn, is an integral of the density field along the beam propagation, and is given by,

$$OPL(x,y,t) = K_{GD} \int \rho(x,y,z,t) dz,$$

where K_{GD} is Gladstone-Dale constant [1]. If the convective speed is known, OPL can be reconstructed from the deflection angle signals using the Taylor frozen field hypothesis [2,3], according to,

[1] Graduate student, Department of Aerospace and Mech. Eng., AIAA Student member.
[2] Associate Professor, Department of Aerospace and Mech. Eng., AIAA Associate Fellow

$$OPL(t = -U_C x) = -U_C \int_{t_o}^{t} \theta(t)dt \ .$$

Thus, by projecting a single small-aperture laser beam through turbulent flows, wavefronts can be directly measured if the convective speed is known. As wavefronts are proportional to the integrated density field, analysis of the time series of deflection angles is very informative way to learn about the underlying turbulent flow. This approach was successfully used to study boundary layers [1,2,4], shear layers [1,5,6], and flows around turrets [3,7,8].

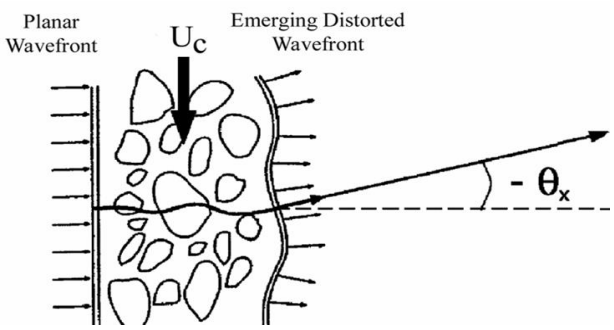

Figure 1: Beam deflection due to turbulent flow.

As a reminder, the regular Malley probe consists of two parallel small-diameter laser beams passing through the tunnel with a small known separation distance in the streamwise direction [2,3]. The resulting jitter or deflection angles imposed on both beams are measured with position-sensing devices (PSDs) or a high-speed digital camera. By cross-correlating the jitter time series, the time delay can be computed, and knowing the distance between the beams, the speed of the flow can be determined [2,3]. A schematic of a conventional Malley probe setup is shown in Figure.

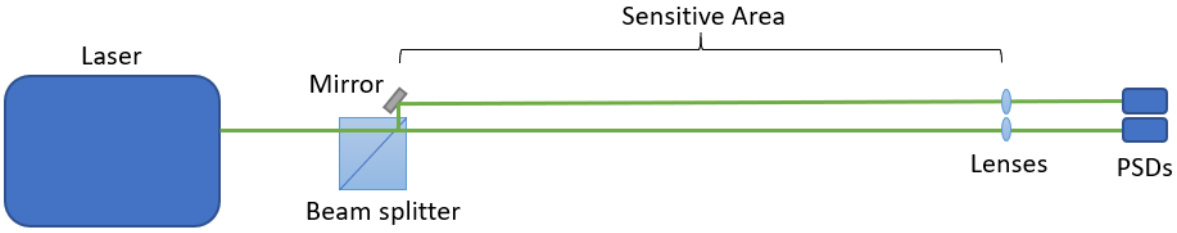

Figure 2: Top-view schematic of a conventional Malley probe.

The issue with this approach is that wavefronts are integrated quantities and do not provide any information about where along the laser beam the optical distortions occur. For spanwise-uniform flows, this problem can be addressed by collecting wavefronts in both wall-normal and spanwise directions [9], but it general it is a drawback of any optical technique involving a collimated laser beam, and results in the inability to determine the exact location of the source of the beam jitter along the beam. This paper seeks to develop a focused version of the Malley probe which is only sensitive to optical distortions in a small, localized measurement region. This would allow for the elimination of distortions due to other contaminating flows along the beam, such as those from tunnel boundary or shear layers, which can become a major issue for measurements in high speed and especially supersonic or hypersonic flows.

Before discussing the proposed focused Malley probe, it is worth mentioning another focused optical technique, known as focused laser differential interferometry, or FLDI [10-13], which also uses a pair of convergent-divergent beams, but uses a different mechanism to achieve a focusing effect. Briefly, FLDI is a non-intrusive local optical measurement technique which

measures the density gradient at the focus location. Because fluctuations in density alter the index of refraction and thus the speed of light through the medium, a density gradient between two nearby points will create different optical path lengths for light traveling through them. If beams that were originally in sync pass through these points, this difference in optical path length will create interference when the beams are recombined on the photodetector, with the variation in intensity proportional to this interference, the difference in optical path lengths, and the density gradient. This method works best when the differences are small enough that the linear approximation along a portion of the sine wave works well, but large enough that it overrides any electronic noise [10].

In order to perform simultaneous measurements of velocity and density gradients, two-point FLDI was developed, which involves using a series of birefringent prisms to create four convergent-divergent beams total, with a small separation near the focal point between the two pairs of beams in order to obtain a cross correlation [14]. In addition to requiring a complex setup with several beams to measure convective velocity, another drawback of FLDI is that it may be affected by variations in ambient light intensity on the sensor.

In contrast, the proposed focused Malley probe may provide the benefit of allowing for local velocity measurements with a much simpler setup only involving two beams and fewer components. While FLDI offers an alternative focused optical technique for local optical measurements, the focused Malley probe could add an additional local aero-optical measurement technique to the toolbox while offering advantages such as the ability to measure convective velocity with a simpler setup. This paper presents the results of measurements with a focused Malley probe in the wake behind a spanwise-mounted cylinder in Mach 0.44 flow.

The concept upon which the focused Malley probe relies to achieve its focusing ability is known as the aperture averaging effect. For a beam passing through turbulent flow, the overall amount of beam jitter measured depends on the beam aperture size. When the beam aperture is large compared to the aberrating optical structures, the contribution to the overall beam deflection is very small due to an aperture-averaging effect, which works as a low-pass filter, effectively suppressing high spatial frequencies present in the wavefronts [7,15]. Figure 3 presents the amount of beam jitter imposed on the laser beam by a turbulent subsonic boundary layer; the overall beam jitter for apertures larger than several boundary layer thicknesses is a hundred times less than for small-sized beams.

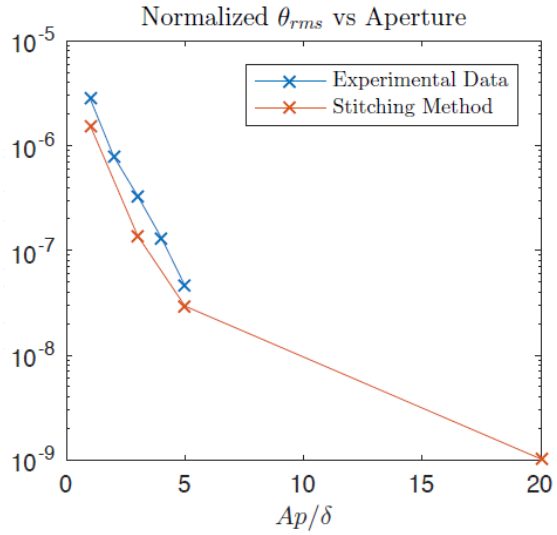

Figure 3: Normalized overall beam jitter due to a boundary layer as a function of the beam size, Ap. From [15].

Previous study [16] has demonstrated the aperture low-pass filtering property, or aperture averaging effect, with constant-diameter laser beams of various apertures passing through the tunnel. This study used a position sensing device,

or PSD, to measure the global jitter for various beam sizes, and demonstrated the effect of larger diameters acting as lower pass filters due to aperture averaging.

In [7] it has been shown that the theoretical ratio of global jitter spectral amplitude to local jitter spectral amplitude in the streamwise direction for one-dimensional periodic wavefront with a characteristic spatial wavelength, Λ, can be expressed through the aperture dependent transfer function, called $G(z)$,

$$G(z) = \frac{\theta_G(f;Ap)}{\theta(f)} = 2[sin(\pi z) - \pi z\, cos(\pi z)]/(\pi z)^3$$

where the parameter $z = {}^{Ap}/_{\Lambda}$ is the aperture diameter divided by the spatial wavelength. For convective structures traveling at the speed of U_c, the spatial wavelength is defined as $\Lambda = U_c/f$, where of convective velocity U_c is approximately 0.82 of U_∞ for subsonic boundary layers [2].

The line-integral aero-optical measurement technique we are seeking to develop a focused version of is the Malley probe. Henceforth, in order to differentiate from the two-beam Malley probe, the taking of jitter measurements from a singular beam shall be referred to as a jitter probe. This paper will focus on the development of the two-beam focused Malley probe, which uses two jitter probes in such a way that two focal point measurements can be taken simultaneously a small distance apart. The development of the focused jitter probe was the subject of the previous paper on this topic [17].

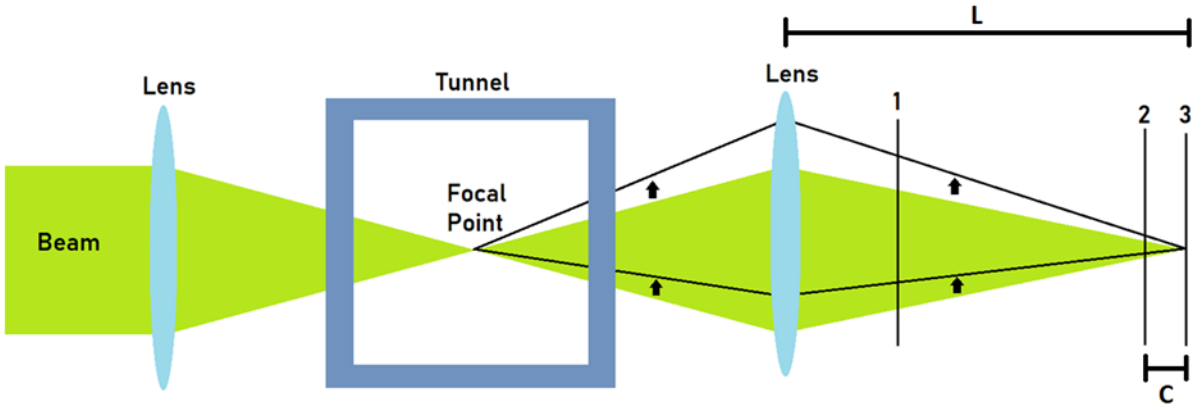

Figure 4: Conceptual schematics of a focused jitter probe. From [17].

The general concept behind a focused jitter probe, which is also used for the focused Malley probe, is shown in Figure 4. A collimated beam with a large diameter is focused to a point inside the tunnel. After the focal point, beam diverges and, after passing through a second focusing lens, is forwarded to a high-speed camera to measure the overall global beam angular deflection. The total beam deflection is an integral of averaged-over-area beam deflections along the beam. Where the beam diameter is large compared to the aberrating optical structures, the contribution to the overall beam deflection is small due to the aperture-averaging effect. Consequently, boundary-layer-related optical effects on both sides of the tunnel windows, while typically large in amplitude, should not significantly contribute to the overall beam deflection. Only the focal point region, where the beam is small, has the largest effect on the total beam deflection. This means that the main contribution to the deflection of the beam occurs primarily along the portion of the

beam near the focal point, where the beam has the smallest diameter. The deflection angles are given by the equations:

$$\theta_x(t) = \frac{\partial OPD(x,y,t)}{\partial x} \approx K_{GD} \frac{\partial}{\partial x} \int \; G(A(z))\rho(x,y,z,t)dz$$

$$\theta_y(t) \approx K_{GD} \frac{\partial}{\partial y} \int \; G(A(z))\rho(x,y,z,t)dz$$

where z is the direction of laser propagation, $A(z)$ is the local aperture and $G(A(z))$ is the aperture-dependent transfer function, which depends on the geometric shape of the beam's cross section and is a function of aperture size. Because the aperture-dependent transfer function greatly attenuates the signal from larger apertures, the deflection angle or overall beam tilt is proportional to the density gradient near the focal point. The aperture-related analysis, provided in [7], assumed that wavefronts are one-dimensional and derived a transfer low-pass function relating small-aperture and large-aperture jitter spectra. As real wavefronts are two-dimensional, the transfer function will be different and depend on wavefront's spatial correlations in both dimensions. This aperture averaging effect has important implications in that it can be used for developing a new way of non-intrusively measuring density fluctuations near the region of the focal point. This measurement technique could be used in hypersonic tunnels, for instance, where the number of measurement techniques are limited due to the need for non-intrusive measurements and the lack of focused techniques that can discern weaker signals in the center of the tunnel from the strong boundary layer signals at the tunnel walls.

The paper on the focused jitter probe has demonstrated that by using a convergent-divergent beam, the focused jitter probe is able to attenuate the contaminating signals from the boundary layers at the tunnel walls in order to discern information about the flow which would have otherwise been obscured by any line-integral measurement technique, such as the conventional jitter probe, which is a single laser beam [17]. This shows that the focused jitter probe behaved as intended, by primarily responding to the boundary-layer aero-optical distortions at the focal point when the point was placed close to either boundary layer, and by reducing the effects of the boundary layer when the focal point was moved away from them to the center of the tunnel. Because the focused Malley probe is essentially two adjacent focused jitter probes, verification of this attenuation capability using converging-diverging beams to take advantage of the aperture averaging effect was essential before proceeding with the dual-beam focused Malley probe.

II. Experimental Set-Up

Experiments were performed using the 100x100 mm transonic in-draft wind tunnel at the Hessert Research Laboratory at the University of Notre Dame. The wind tunnel test section has optical quality glass installed on the sides where the laser beam was transmitted through. A variable intensity 532 nm YaG:Nd laser was expanded to 25.4 mm using a beam collimator. Then, the beam was spit using a beam splitter, with the spit beam directed using a mirror so that both beams converge on the first lens with a small difference in incident angle of approximately 1.3^o, as shown in Figure 5. Additional turning mirrors, not shown, were used to allow the setup to fit on the

breadboard while achieving a small difference in incident beam angle. This small angle created two focal points of separation S = 5.15 mm apart when the beams were converged using the 225 mm focal length lens. The small region around these focal points where the beam apertures are small is the local focused measurement region of the sensor, and this measurement region can be translated to various locations within the wind tunnel. The test section used had a 3.175 mm diameter cylinder mounted vertically in the center to create additional localized optical distortions in the tunnel. A 150 mm focal length lens was used after the tunnel to re-converge the beams to a Phantom v1611 high speed camera. Varying the position of this second lens simultaneously varies the final focusing distance 'L', defined in Figure 4, as well as the spot separation distance on the camera sensor. Closer spots on the camera sensor allow for a higher sampling frequency. A neutral density (ND) filter was used to reduce the intensity of laser light going into the camera.

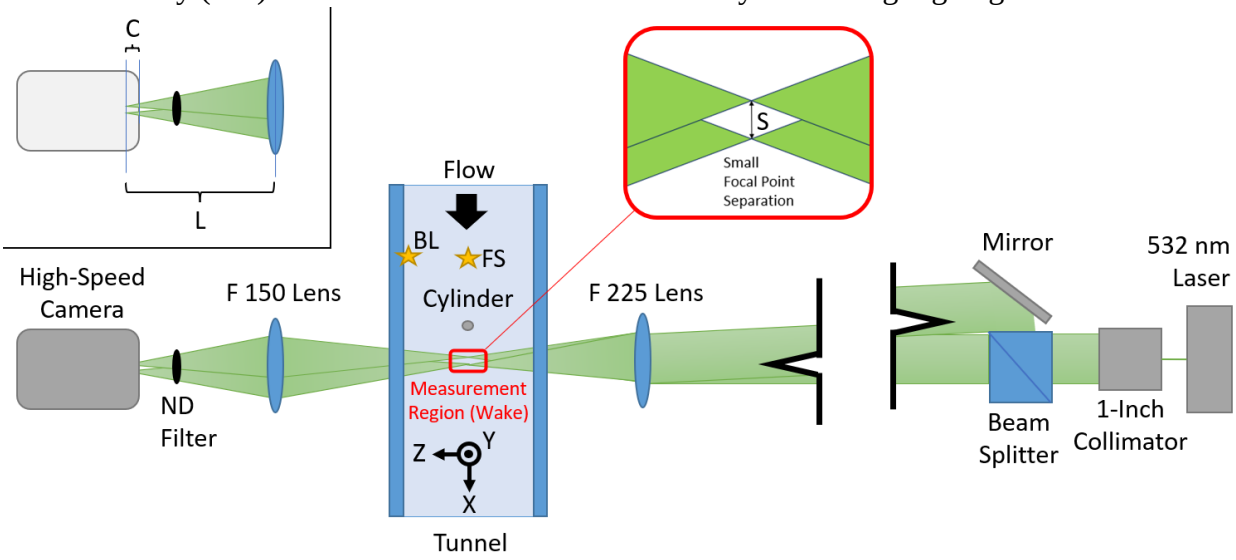

Figure 5: Top-view schematic of experimental set-up for cylinder wake measurements with the focused Malley probe.

Looking back at Figure 4, it is important to note that due to reimaging, deflections at the focal point will result in zero beam shift at position 3, so a sensor cannot be placed here to measure deflections. For this reason, in order to perform focused jitter measurements, the sensor must measure the beam displacement some distance away from the focal point, such as position 2, but not so far away that the beam would be so large that a high-speed camera could not measure it at high frequency, such as would be the case with position 1. The distance the camera is placed away from the focal point, denoted as C, can be modified as a fraction of the total distance to the focusing lens, denoted as L in Figures 4 and 5, and this fraction is referred to as the C/L ratio. Clearly, the beam displacement magnitude is proportional to C/L ratio, so larger values of C/L result in a stronger signal. On the other hand, the beam size is also proportional to the C/L ratio, resulting in a larger image size and, consequently, a smaller sampling frequency. In [17] a parametric analysis was performed, and it was demonstrated that the values of C/L between 15% and 25% are optimal to achieve both a strong signal and sufficient sampling frequency in order to properly resolve the localized jitter spectrum.

Experiments were conducted by placing the measurement region at three different locations within the test section at a Mach number of 0.44, to measure the signals from the wake of the cylinder, the free stream, and the boundary layer. The first set of experiments, illustrated in Figure 5, were conducted with the focal points approximately 5.5 cylinder diameters downstream of the cylinder in the wake region, and the other two sets of experiments were performed with the focal points approximately 9.5 cylinder diameters upstream of the cylinder, with the second set focused on the free stream flow in the center of the tunnel, and the third set focused on the left turbulent boundary layer, with the focal points roughly one third the boundary layer thickness of 15.6 mm away from the tunnel wall. The location of the measurement region for the free stream is denoted as 'FS' and the location of the measurement region for the boundary layer is denoted as 'BL' in Figure 5. The cylinder formed a turbulent wake with vortex shedding at a theoretical frequency of $St_D = 0.2$ [18] or 9.55 kHz. Experiments were performed with C/L ratios of 5% and 20% for all focal point locations, with additional measurements performed with C/L ratios of 10% and 15% in the wake of the cylinder. The final distance 'L' was 405 mm, or in one case 425 mm, for a ratio of 20%, 285 mm for 15%, and 250 mm for both 10% and 5%. The complete test matrix for all experiments conducted using the focused Malley probe is shown in Table 1.

Table 1: Test Matrix for Focused Malley Probe Experiments

Case Number	Measurement Location	C/L Ratio	Sampling Frequency (kHz)	Final Distance L (mm)
1	Cylinder's Wake	20%	110	425
2	Cylinder's Wake	20%	150	405
3	Cylinder's Wake	15%	220	285
4	Cylinder's Wake	10%	320	250
5	Cylinder's Wake	5%	720	250
6	Cylinder's Wake	5%	150	250
7	Free Stream	20%	150	405
8	Free Stream	5%	720	250
9	Free Stream	5%	150	250
10	Boundary Layer	20%	150	405
11	Boundary Layer	5%	720	250
12	Boundary Layer	5%	150	250

III. Data Reduction

Beam displacement data was recorded using a Phantom v1611 high speed camera. The beams were converged to small diameter spots on the camera from which the displacements could be directly extracted, taking care to avoid the attenuation at the exact focal point. The camera was placed at various distances way from the final lens in order to determine the effect of this distance on the spot quality and spectral quality. Assuming a small angle approximation, the beam displacement readings, x, illustrated in Figure 6, were divided by the distance C in order to find the beam angular displacement a_1, otherwise referred to as the global beam jitter, at the sensor location. Small angle approximations were then used to determine a scale factor to convert the

angular displacement a_1 at the sensor location to the angular displacement a_2 at the measurement location, or the pair of focal points inside the tunnel. If the final focusing distance after the second lens is defined as L_1 and the distance between the measurement location focal points inside the tunnel and the second lens is defined as L_2, then using the equal deflection distance at the second lens h, this scale factor to convert sensor-location angular deflections to measurement-location angular deflections is equal to L_1/L_2. Because L_1 is directly measured during the experiment and the second-lens focal length of 150 mm is known, L_2 can be determined from the thin lens equation.

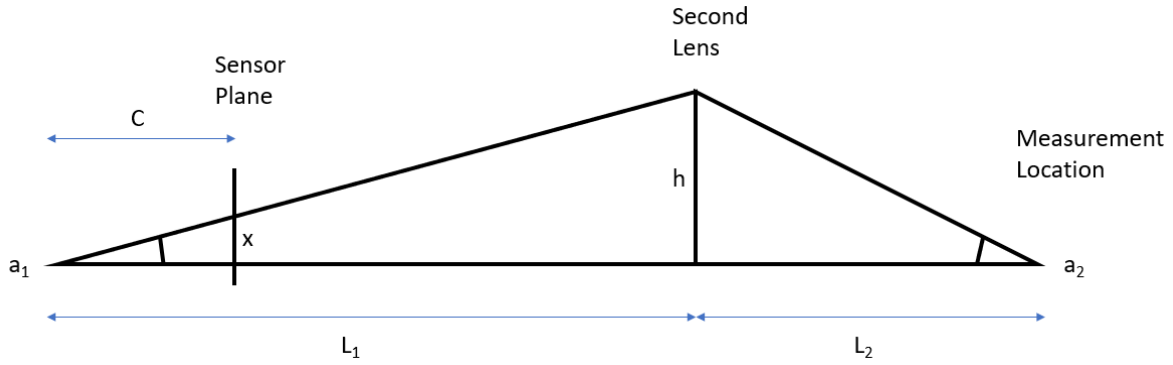

Figure 6: Schematic for Calculation of Scale Factor for Deflection Angles

Obtaining reliable beam displacement data with the focused jitter probe requires an extra step of processing which is not required with the traditional Malley probe. All existing aero-optical measurement techniques using lasers typically rely on focusing the beam down to a small point to measure the overall centroid position of that point, and this act of focusing to a point tends to get rid of the effects of any intensity variations within the beam itself that do not affect the overall centroid motion.

The intensity-based method for determining the centroid of the beam, which is the standard for aero-optical measurements, consists of taking a weighted average centroid of the image, calculated by the equation below, based on the intensity of each pixel at each instant in time. In this equation, p represents the pixel, x_p is the x-location, or y-location, depending on the direction chosen, of the pixel on the sensor, I_p is the intensity of the pixel, and N is the total number of pixels.

$$x_{centroid}(t) = \frac{\sum_{p=1}^{N} x_p I_p}{\sum_{p=1}^{N} I_p}$$

However, with larger spots, as is the case with the focused Malley probe or focused jitter probe, intensity variations inside the spot due to diffraction patterns from dust and other optical imperfections tend to affect the measurement, so additional processing must be done in order to determine the best way to capture the overall motion of the spot. The paper on the focused jitter probe goes into detail on the need for applying a thresholding algorithm to each image before computing the centroid [17]. This threshold value should be chosen individually for each of the two spots in each data set in order to minimize the number of dark pixels within the spot and bright pixels outside of the spot. A mask is applied to each spot to compute the centroids of the left and

right spots individually. Once the threshold is applied to each spot, the same centroiding algorithm from the equation above is applied to compute the spot centroid at each instant in time. Examples of the unthresholded spots for the simultaneous measurement of the upstream and downstream beams for the focused Malley probe for C/L ratios of 20% and 5% are shown below in Figures 7 and 8, respectively. Due to their inability to perform image thresholding, position sensitive devices (PSDs) cannot be used for the focused Malley probe because of their sensitivity to the spatial intensity variation. For this reason, a high-speed camera must be used to capture the full images for post-processing.

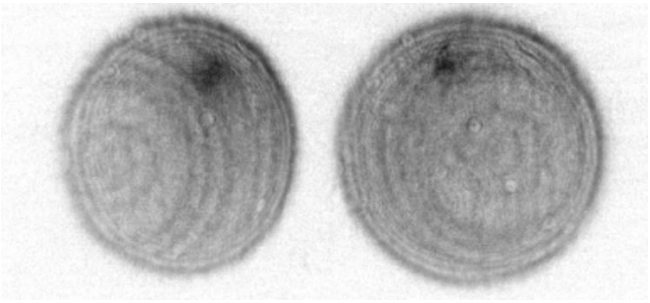

Figure 7: Unthresholded inverted-color upstream an downstream spot patterns for focused Malley probe at a C/L ratio of 20%.

Figure 8: Unthresholded inverted-color upstream and downstream spot patterns for focused Malley probe at a C/L ratio of 5%.

Similar to the conventional Malley probe data analysis [3], the cross-correlation spectral analysis was implemented to compute the time delay between the two beams. After converting the beams' displacements into the global angular deflections or jitter at the measurement region, the mean of each global beam jitter was removed, and the jitter power spectra were computed using a standard block averaging Fourier transform. The cross spectral density, S(f), between the two beams was computed using standard block averaging Fourier transforms with a Hanning window and 500 blocks. The general equation for cross spectral density S(f) is given below, where C(ω) is the Fourier transform of the deflection angles inside the tunnel x(t) and T is the time period. C*(ω) represents the conjugate.

$$C(\omega) = \int_{-\infty}^{\infty} x(t) e^{-i\omega t} dt$$

$$S(f) = \frac{C^*_{upstream}(\omega) C_{downstream}(\omega)}{2\pi T}$$

The phase of the cross spectral density function was then computed, and the phase was unwrapped to compute the linear fit. For a quality data set, the unwrapped phase plot should show

an identifiable slope related to the time delay, τ, of the convecting optical structures by the equation below.

$$\tau = \frac{1}{2\pi}\frac{d}{df} phase[S(f)]$$

In order to determine the slope, linear regions of the unwrapped phase plots were visually identified, and linear fits were performed over the appropriate frequency ranges. Some data sets showed linear slopes as expected, while others showed no meaningful signal and were corrupted by noise, as discussed later on. The R^2 value of the linear fit was determined to gauge the quality of the correlation and the fit, and is given by the equation below.

$$R^2 = 1 - \frac{\sum_i (phase(f)_i - fit(f)_i)^2}{\sum_i (phase(f)_i - \overline{phase(f)})^2}$$

Once the time delay is known, it can be used along with the known separation between the two beams at the measurement location, defined as 's' in Figure 5, which is 5.15 mm for these experiments, to compute the local convective velocity U_C according to the equation $U_C = s/\tau$. The ambient temperature can then be used to determine the speed of sound, and the free stream speed was estimated to be U_∞ = 152 m/s for these experiments from the known Mach number of M = 0.44, measured by using a Pitot probe installed in the test section upstream of the cylinder. The freestream speed can then be used to determine the ratio U_C/U_∞.

IV. Results and Discussion

In order to obtain an accurate measurement for the separation between the two focal points at the measurement location inside the tunnel, the high-speed camera was moved in place of the test section and translated to have these focal points on the camera sensor. The separation between these focal points was then measured in pixels and converted to meters. This separation distance of 5.15 mm was kept constant throughout the experiments, with the exeption of Case 1 at 110 kHz, which was taken earlier and had the spot separation measured to 5 mm with a ruler.

The streamwise jitter power spectra for both beams of the focused Malley probe for Case 1 with a C/L ratio of 20% is shown in Figure 9 (left). The spectrum taken from a conventional jitter probe, consisting of a small aperture laser beam, is shown for comparison. It should be noted that this was the only test case without the focal point separation distance measured precisely with the camera. While there is a noise floor and some spikes due to noise, the peaks at twice the vortex shedding frequency of 19 kHz and to a lesser extent the peaks at the vortex shedding frequency of 9.5 kHz are clearly resolved by the focused Malley probe. The peak at twice the vortex shedding frequency is much stronger, as expected, due to vorticies shedding off both sides of the cylinder and mixing in the wake. This effect was also observed in the previous experiments for the same flow with the focused jitter probe [17]. As it will be shown later, the signal from these two peaks is still sufficient to obtain a cross-correlation between the two focal points for a convective velocity measurement. For runs with large C/L ratios and lower sampling frequencies, the global jitter

spectra also exhibit signs of aliasing above 20 kHz. This is due to the lower sampling frequency of the focused Malley probe with large C/L ratios compared to the convetional jitter probe.

For the phase plot for Case 1 shown in Figure 9 (right), there is a clearly visible slope trend from around zero to 40 kHz, which is also consistent with other test cases, and this frequency range was used to compute the linear fit over the unwrapped phase for all test cases unless stated otherwise. The R^2 value of 0.92 for the linear fit shows a high degree of correlation, and the phase slope yielded a convective velocity of 125 m/s and a U_C/U_∞ ratio of 0.826. This value of the convective speed is consistent with the expected value of the convective speed in the wake downstream of the cylinder of about 0.8-0.9 of the freestream speed.

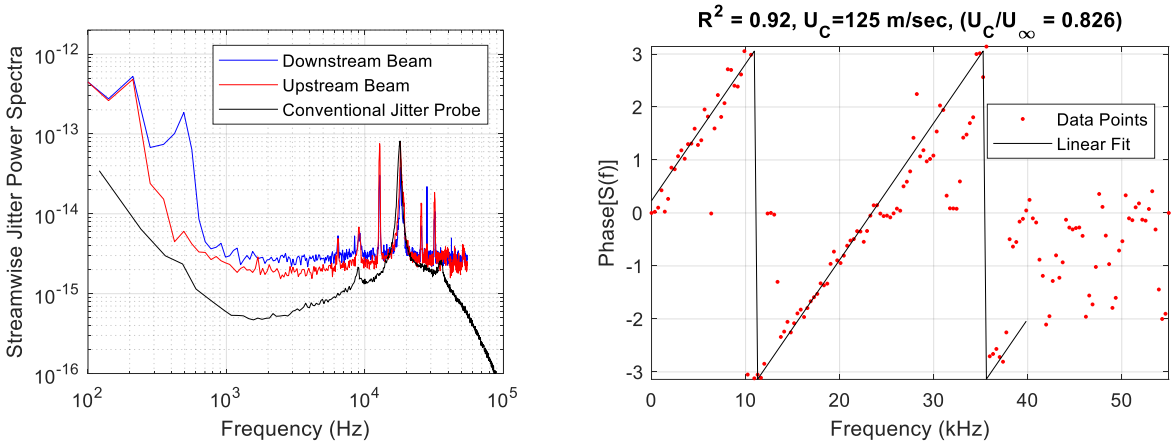

Figure 9: Case 1, Focused Malley probe streamwise jitter power spectra (left) and phase plot (right) for Mach 0.44 flow 5.5 diameters downstream of cylinder, with a C/L ratio of 20% and L = 425 mm, sampled at 110 kHz.

The streamwise jitter spectra and phase plots for Case 2 at a C/L ratio of 20% are shown in Figure 10. There are more points deviating from the fit than for Case 1, but there is still a clear slope trend visible in the selected frequency range. It is worth noting that the points which deviate from the slope trend tend to be at the same frequency as the spikes at the vortex shedding frequency and twice the vortex shedding frequency. At these frequency values, for both test cases with C/L ratios of 20%, the phase goes to zero. Frequencies with zero phase values usually indicte the presence of mechanical contamination, and the observed zero phases may be due to shedding-related vibrations at these frequencies being imposed on the tunnel glass. The R^2 value was 0.89 for the linear fit, and the phase slope yielded a convective velocity of 138 m/s and a U_C/U_∞ ratio of 0.907, which is similar to the value computed for Case 1.

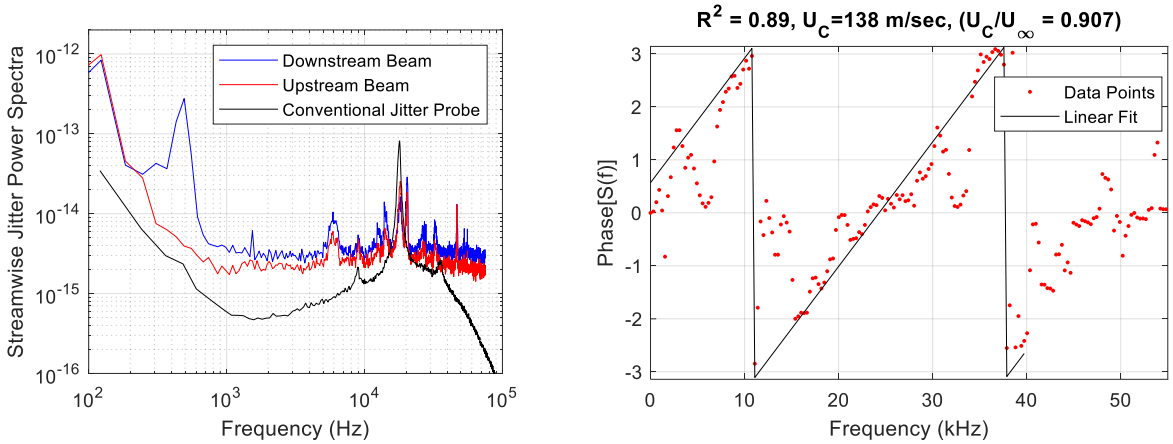

Figure 10: Case 2, Focused Malley probe streamwise jitter power spectra (left) and phase plot (right) for Mach 0.44 flow 5.5 diameters downstream of cylinder, with a C/L ratio of 20% and L = 405 mm, sampled at 150 kHz.

Figure 11 shows the spectra and the phase plots for a lower ratio of C/L ratio of 15%. At this ratio, there are some significant noise spikes present in the jitter spectra, as shown in Figure 11 (left), at higher frequencies, which likely contributed to the deviation at higher frequencies in the phase plot shown in Figure 11 (right), but the spikes in the spectra at the vortex shedding frequency and twice the vortex shedding frequency are still strong enough to provide a clearly visible slope in the phase plot up to around 40 kHz.

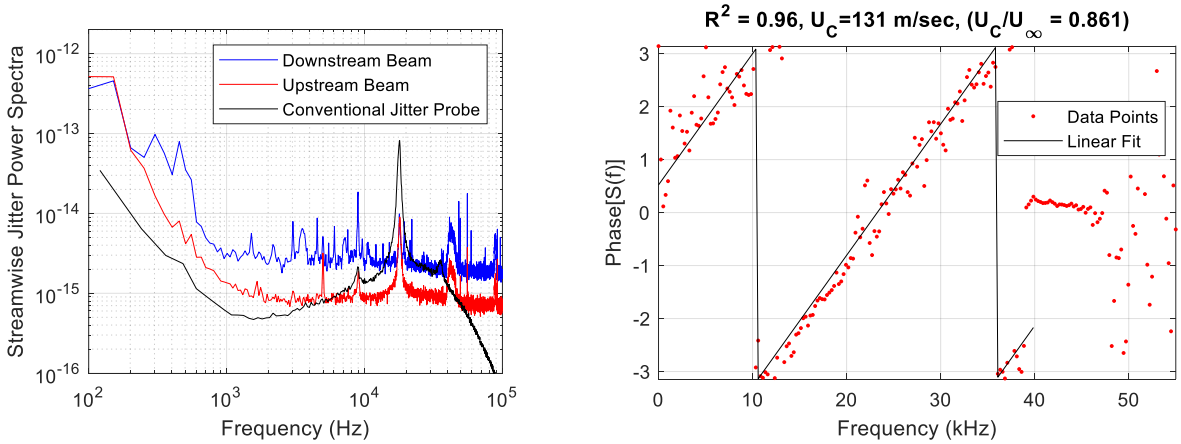

Figure 11: Case 3, Focused Malley probe streamwise jitter power spectra (left) and phase plot (right) for Mach 0.44 flow 5.5 diameters downstream of cylinder, with a C/L ratio of 15% and L = 285 mm, sampled at 220 kHz.

The amplitude discrepancy between the upstream and downstream beam spectra is likely due to differing noise floors in the spot centroid calculations, as each individual spot had slight variations and individually selected thresholding values. While thresholding greatly mitigates the effects of interference patterns, there are bound to still be some effects form interference at the edge of the thresholding range, and these effects will be unique to each spot, potentially resulting in a different amplitude for the noise floor between the spots for the upstream and downstream

beams for each test case. Potential ways to reduce this noise floor for future experiments will be discussed in the next section. For this case, the R^2 value of the linear fit was 0.96, with a value for the convective velocity of 131 m/s and a U_C/U_∞ ratio of 0.861, consistent with the values for Cases 1 and 2.

Figure 12 shows the streamwise jitter power spectra and phase plot for Case 5, taken downstream of the cylinder at an even lower C/L ratio of 5% and a sampling frequency of 720 kHz. As can be seen from the jitter spectra in Figure 12 (left), the spikes at the vortex shedding frequency and twice the vortex shedding frequency are both visible, which leads to a slope from the signal visible in the phase plot, shown in Figure 12 (right), up to 23 kHz, but no linear phase slope is visible at higher frequencies. This is expected, as the noise floor in the spectra overrides any flow signal at these higher frequencies, since the spikes due to vortex shedding, which are the flows of interest, are only present at lower frequencies. There is a steep drop-off in the unwrapped phase, which is used to compute the slope, above 23 kHz, so for this test case, only the frequency range below this value was used to compute the slope in order to not introduce error from noise into the calculation. This increased noise is likely due to the fact that the lower signal magnitude for the C/L ratio of 5% is smaller compared to the constant camera pixel size across all C/L ratios, which would result in more noise relative to the signal. The amplitude discrepancy between the upstream and downstream spectra in Figure 12 (left), is likely due to differing noise floors for each individual spot, as discussed earlier. Aliasing is not likely the cause of the flat spectra at the high end of the frequency range due to the high sampling frequency of 720 kHz, and this effect is likely due to the noise floor for each spot. As a result of the increased noise, the linear fit for Case 5 had an smaller value R^2 value of 0.82, with the convective velocity of 140 m/s and a U_C/U_∞ ratio of 0.923.

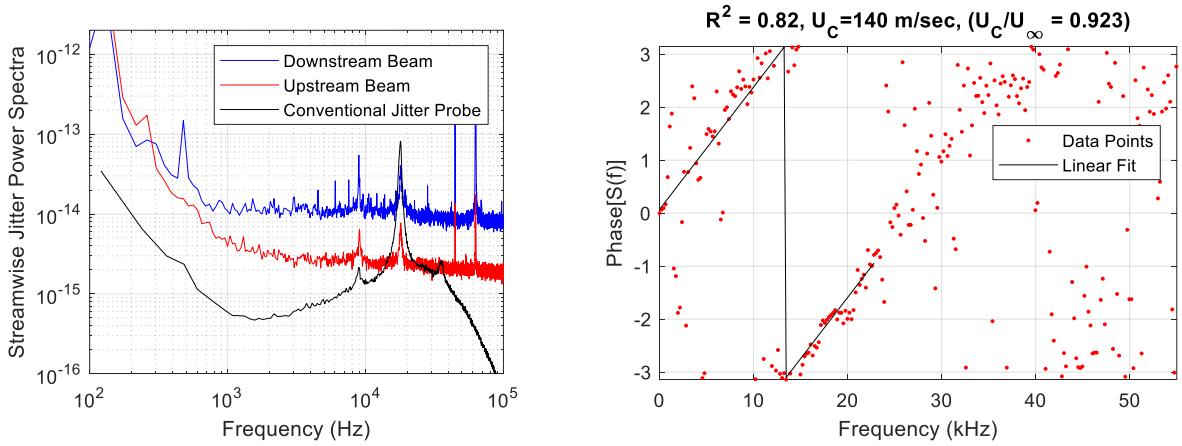

Figure 12: Case 5, Focused Malley probe streamwise jitter power spectra (left) and phase plot (right) for Mach 0.44 flow 5.5 diameters downstream of cylinder, with a C/L ratio of 5% and L = 205 mm, sampled at 720 kHz.

For all of the measurements taken with the focal points placed in the freestream in the center of the tunnel approximately 9.5 cylinder diameters upstream of the cylinder, Cases 7-9, there was no noticable slope to obtain any measurement from on any of the phase plots. For example, Figure 13 shows the jitter spectra and phase plot for Case 7, taken in the free stream at a C/L ratio of 20%. As can be seen from the very low R^2 value of 0.069 and the non-physical U_C/U_∞

ratio well above one, there is no meaningful correlation or noticable slope in this phase plot, as any signal that may be present is overridden by noise. This is expected, since the freestream region does not have any strong density fluctuations and, consequently, does not create any strong optical distortions.

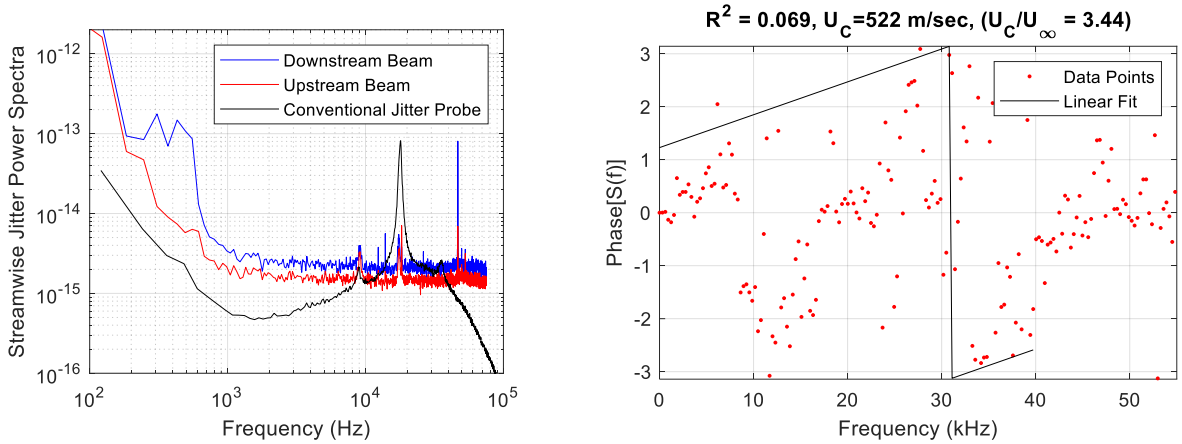

Figure 13: Case 7, Focused Malley probe streamwise jitter power spectra (left) and phase plot (right) for Mach 0.44 flow 9.5 diameters upstream of cylinder centered in the free stream, with a C/L ratio of 20% and L = 405 mm, sampled at 150 kHz.

For the measurements taken with the focal points placed in the turbulent boundary layer approximately 9.5 cylinder diameters upstream of the cylinder, only test Case 10, shown in Figure 14, with a C/L ratio of 20%, yielded a phase plot with a well-defined slope due to the strong flow signal. This slope was visible up to a frequency of around 40 kHz, as with most of the cases with a visible slope for the cylinder's wake, and for Case 10 the R^2 value was 0.85 for the linear fit. The resulted convective velocity of 178 m/s and a U_C/U_∞ ratio of 1.17. Because this ratio should theoretically be around 0.82 for a turbulent boundary layer, this discrepancy is likely due to noise obscuring the signal, and potential sources of error as well as potential areas of improvement which could help alleviate such issues in future iterations will be discussed in the following section.

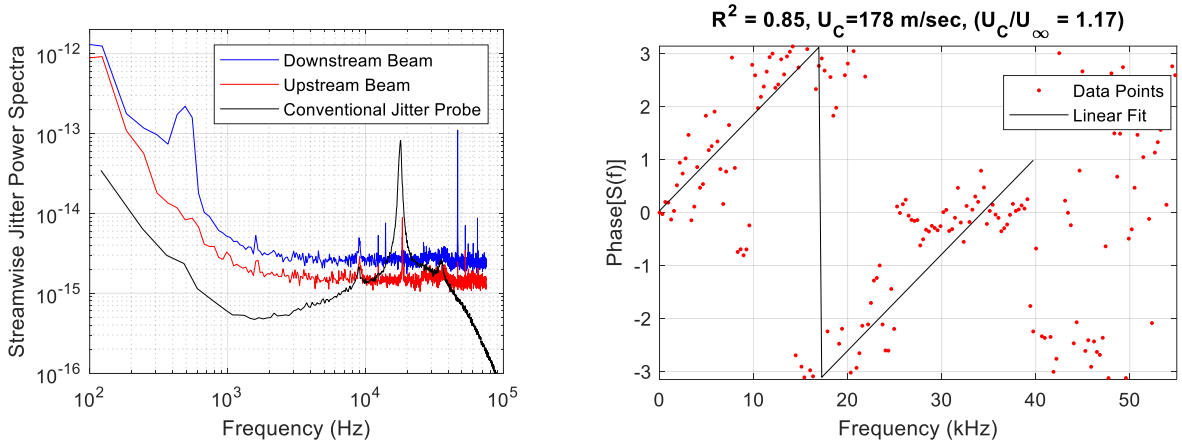

Figure 14: Case 10, Focused Malley probe streamwise jitter power spectra (left) and phase plot (right) for Mach 0.44 flow 9.5 diameters upstream of cylinder in the turbulent boundary layer, with a C/L ratio of 20% and L = 405 mm, sampled at 150 kHz.

The results for all test cases which yielded well-defined slopes on the phase plots, along with a representative test case for the free stream, are summarized in Table 2. All of the linear fits had a high degree of correlation with an R^2 value above 0.8, and for larger C/L ratios of 15% and 20% taken in the wake of the cylinder, the linear fits had an even higher correlation with R^2 values of around 0.9 and above. For Case 1, the measurement region focal point separation was measured with a ruler, resulting in larger uncertainty in the distance between the focal points. For Cases 2, 3, and 5, where this separation was measured more accurately using the camera, the mean value of the convective to free stream velocity ratio was 0.897, and all three values fall within 4% of this mean, showing there is fairly good agreement across C/L ratios for measurement of the convective velocity in the wake of the cylinder. There was virtually no correlation for the freestream in Case 7, as expected, due to the optical signal near the focal points being too weak to be measurable, although future improvements to reduce this noise floor are possible. Although the boundary layer phase plot for Case 10 yielded a discernable slope which resulted in a convective velocity on the correct order of magnitude, the current noise floor was also an issue here, and resulted in a significant discrepancy between the measured value for the ratio of 1.17 and the expected value of 0.82. Overall, there are improvements that can be made to reduce the noise floor, but the good agreement between Cases 2, 3, and 5 in measuring the convective velocity in the wake of the cylinder serves as a proof of concept for the focused Malley probe as a novel local non-intrusive aero-optical wavefront measurement technique.

Table 2: Summary of U_C/U_∞ Results for Experiments with the Focused Malley Probe

Case Number	Measurement Location	C/L Ratio	R^2 of Linear Fit	Convective Velocity U_C (m/s)	Ratio $U_C/U\infty$
1	Cylinder's Wake	20%	0.92	125	0.826
2	Cylinder's Wake	20%	0.89	138	0.907
3	Cylinder's Wake	15%	0.96	131	0.861
5	Cylinder's Wake	5%	0.82	140	0.923
7	Free Stream	20%	0.069	-	-
10	Boundary Layer	20%	0.85	178	1.17

V. Conclusions and Future Work

This paper presented some preliminary measurements of localized aero-optical distortions using a novel non-intrusive local aero-optical wavefront measurement technique, termed the focused Malley probe. The probe consisted of two convergent-divergent laser beams, with focal points separated by a known distance in the streamwise direction. Global beam jitter of both beams were simultaneously measured using a high-speed camera, and the spectral cross-correlation analysis was implemented to extract the jitter spectra and the convective speed of the aero-optical structures near the focal points. It was demonstrated that the focused Malley probe is capable of correctly measuring the local jitter spectra and the related convective speed of the aero-optical structures near the focal points while suppressing aero-optical signal everywhere else via the aperture averaging effect. Measurements were performed with the focal points been placed in the

wake behind a cylinder, in the free stream ahead of the cylinder, and in the wall turbulent boundary layer ahead of the signal. For the measurements in the wake of a cylinder where the focal point separation was measured accurately with the camera, C/L ratios of 20%, 15%, and 5% gave consistent convective velocity measurements within 4% of the mean and the expected convective speed. While the ratio of C/L = 5% also resulted in a reasonable estimate of the convective speed in the wake of the cylinder, the uncertainty of the measurements was higher due to the much lower signal magnitude of this lower C/L ratio resulting in a higher noise floor. No usable signal was measured above the noise level in the freestream region for any C/L ratio, and only one test case produced a noticeable phase slope due to the flow on the phase plot for the measurements of the turbulent boundary layer, but even this measurement had significant error. Despite these areas for improvement, the experiments in the wake behind the cylinder at C/L ratios of 20%, 15%, and 5% serve as a proof of concept that the focused Malley probe can be used to measure both streamwise jitter spectra and the convective velocity of the flow near the focal points.

Future studies will more closely study and address several sources of error which may be contributing to the noise interfering with the signal. One potential source of error which could be improved is the geometry of the beam setup. As shown in the setup in Figure 5, both incident beams with small separation angle are centered on the first lens, but have an appreciable separation on the second lens, meaning they were not going through the center of the lens, which resulted in aberrations in the final spot shapes, so they were not perfectly round. This effect could be mitigated by having more of a balance between the spot separations on the first and the second lenses to try and mitigate these aberrations. Another potential source of error is the relatively small final focusing distance L for all of the runs, which may have resulted in additional aberrations. Choosing different lenses and a setup which would result in a longer final focusing distance should help mitigate these aberrations. In addition, the focal spot separation inside the tunnel could be adjusted to test the effect of different values for this parameter on the ability to obtain quality measurements. Overall, there are several areas for further testing, improvement, and refinement of this novel aero-optical measurement technique, but these first experiments in the wake of a cylinder serve as a proof of concept for the focused Malley probe.

References

[1] S. Gordeyev, E.J. Jumper, “Physics and Measurement of Aero-Optical Effects: Past and Present,” Annual Review of Fluid Mechanics, **49**, pp. 419–441, 2017.

[2] S. Gordeyev, A. E. Smith, J.A. Cress and E.J. Jumper, “Experimental studies of aero-optical properties of subsonic turbulent boundary layers," *Journal of Fluid Mechanics*, **740**, pp. 214-253, 2014.

[3] S. Gordeyev, T. Hayden and E. Jumper, "Aero-Optical and Flow Measurements Over a Flat-Windowed Turret", *AIAA Journal*, **45**(*2*), pp. 347-357, 2007.

[4] S. Gordeyev, J.A. Cress, A Smith and E.J. Jumper, " Aero-optical measurements in a subsonic, turbulent boundary layer with non-adiabatic walls", Physics of Fluids, 27, 045110, 2015.

[5] Malley M, Sutton GW, Kincheloe N. 1992. Beam-jitter measurements of turbulent aero optical path differences. Appl. Opt. 31:4440–43.

[6] Fitzgerald, E., and Jumper, E. (2004). The optical distortion mechanism in a nearly incompressible free shear layer. Journal of Fluid Mechanics, 512, 153-189.

[7] N. De Lucca, S. Gordeyev, and E. Jumper, "The Study of Aero-Optical and Mechanical Jitter for Flat-Windowed Turrets", AIAA Paper, 2012-0623.
[8] B. Vukasinovic, A. Glezer, S. Gordeyev, E. Jumper and V. Kibens, "Fluidic Control of a Turret Wake: Aerodynamic and Aero-Optical Effects", AIAA Journal, Vol. 48,No, 8, pp. 1686-1699, 2010.
[9] J. Sontag and S. Gordeyev, "Non-intrusive Velocity and Density Measurements in Subsonic Turbulent Boundary Layer ", AIAA Paper 2015-3247, 2015.
[10] B. E. Schmidt and J. E. Shepherd. "Analysis of Focused Laser Differential Interferometry." Applied Optics, 2015.
[11] Matthew R. Fulghum. "Turbulence Measurements in High-Speed Wind Tunnels Using Focusing Laser Differential Interferometry." Pennsylvania State University, 2014.
[12] N. J. Parziale, J. E. Shepherd, and H. G. Hornung. "Observations of Hypervelocity Boundary-Layer Instability." Journal of Fluid Mechanics, Cambridge University Press, 2015.
[13] N. J. Parziale, J. E. Shepherd, and H. G. Hornung. "Differential Interferometric Measurement of Instability in a Hypervelocity Boundary Layer." AIAA Journal 51:3, 2013.
[14] A. Ceruzzi and C.P. Cadou, "Simultaneous Velocity and Density Gradient Measurements using Two-Point Focused Laser Differential Interferometry," *AIAA*, 2019.
[15] M.R. Kemnetz and S. Gordeyev, "Multiple aperture approach to wavefront prediction for adaptive-optic applications," AIAA Paper 2017-1344, 2017.
[16] L. Butler and S. Gordeyev, "Effect of Varying Beam Diameter on Global Jitter of Laser Beam Passing Through Turbulent Flows", AIAA Paper 2019-3385, 2019.
[17] L. Butler and S. Gordeyev, "Local Aero-Optical Measurements of a Wake behind a Cylinder in Turbulent Flow using a Focused Jitter Probe." AIAA Paper 2021-0937, 2021.
[18] A.E. Potts, D.A. Potts, H. Marcollo, and K. Jayasinghe, "Strouhal Number for VIV Excitation of Long Slender Structures", ASME, No. OMAE2018-77433, V005T04A073, 2018.